Chapter 6: Other Experiments

6.1 Space-charge Coupling of Transverse Dimensions

Liouville's theorem states that for a Hamiltonian system of N particles, the 6N-dimensional phase space density is a constant of the motion. For non-interacting particles, one may integrate over all but one of the particles and obtain a single-particle 6-dimensional distribution function, which is also a constant of the motion. For charged particles, inclusion of the self-fields complicates matters because of direct collisions between particles. In this experiment, discrete collisional effects are entirely negligible, and the distribution may be described in a 6-dimensional phase space.

To the degree that the spatial dimensions are decoupled, each may be described by averaging over the others and obtaining 2-dimensional distributions. This is standard practice in accelerator physics. The longitudinal dimension is usually decoupled from the transverse dimensions, and the two transverse dimensions are independent of each other to the degree that the lenses are linear and orthogonally well aligned. The space-charge coupling of the beam radius in the two dimensions does not affect this condition in the ideal, linear-field case. However, non-linear space-charge fields can provide coupling in phase space. (Such coupling between dimensions is introduced externally in electron storage rings, through use of skew quadrupoles, to communicate the cooling effects of synchrotron radiation between the horizontal and vertical planes.) In the case of uncorrelated distributions in the x and y planes, the product of the emittances in the two planes should either be constant or grow somewhat.

That space-charge fields can provide this coupling is demonstrated by the following experiment. A single parallel-wire terminating grid had been placed at the ion gun output, with the wires oriented at 45° from the quadrupole

planes. The emittances in the vertical and horizontal planes were measured along the lattice and found to be equal at each lattice position and approximately constant in z. We then oriented the wires horizontally, and repeated the measurements. The field due to the image charges on the grounded grid wires was almost exclusively in the vertical plane, so that the emittance in the vertical plane received the entire grid perturbation, while the horizontal dimension retained the intrinsic source emittance. (A detailed discussion of grid effects on emittance is given in Appendix C.) The ratio of the emittances in the two planes as measured after Q4, a short distance downstream from the source, was about 2:1, vertical:horizontal.

The results of the experiment are shown in Figs. 6.1 and 6.2. The emittances in the two planes are coupled, equilibrating with a characteristic distance of approximately 15 periods or less. The emittances as measured at Q35, about 15 periods downstream from the Q4 measurement point, are nearly equal. The emittance in the vertical plane is still somewhat larger than that in the horizontal plane. But by the time the beam arrives at the end of the lattice, the emittances in the two planes are equal. In the absence of a strong x–y asymmetric instability, then, we expect that ϵ_x and ϵ_y will be nearly equal for space-charge dominated beam transport. This may affect any HIF scenario involving beam merging.

If the interaction redistributes the beam transverse kinetic energy, without coupling in any of the electrostatic or longitudinal kinetic energy, then the sum of the squares of the RMS emittances will be constant. In this case, then the product of the two emittances will grow. However, because the initial ratio of the emittances in the two planes is only about 2, we cannot distinguish between the conservation of the product, simple sum, or the sum of the squares of the emittances in the two planes. Conservation of these quantities, respectively, for an initial ratio between the x and y emittances

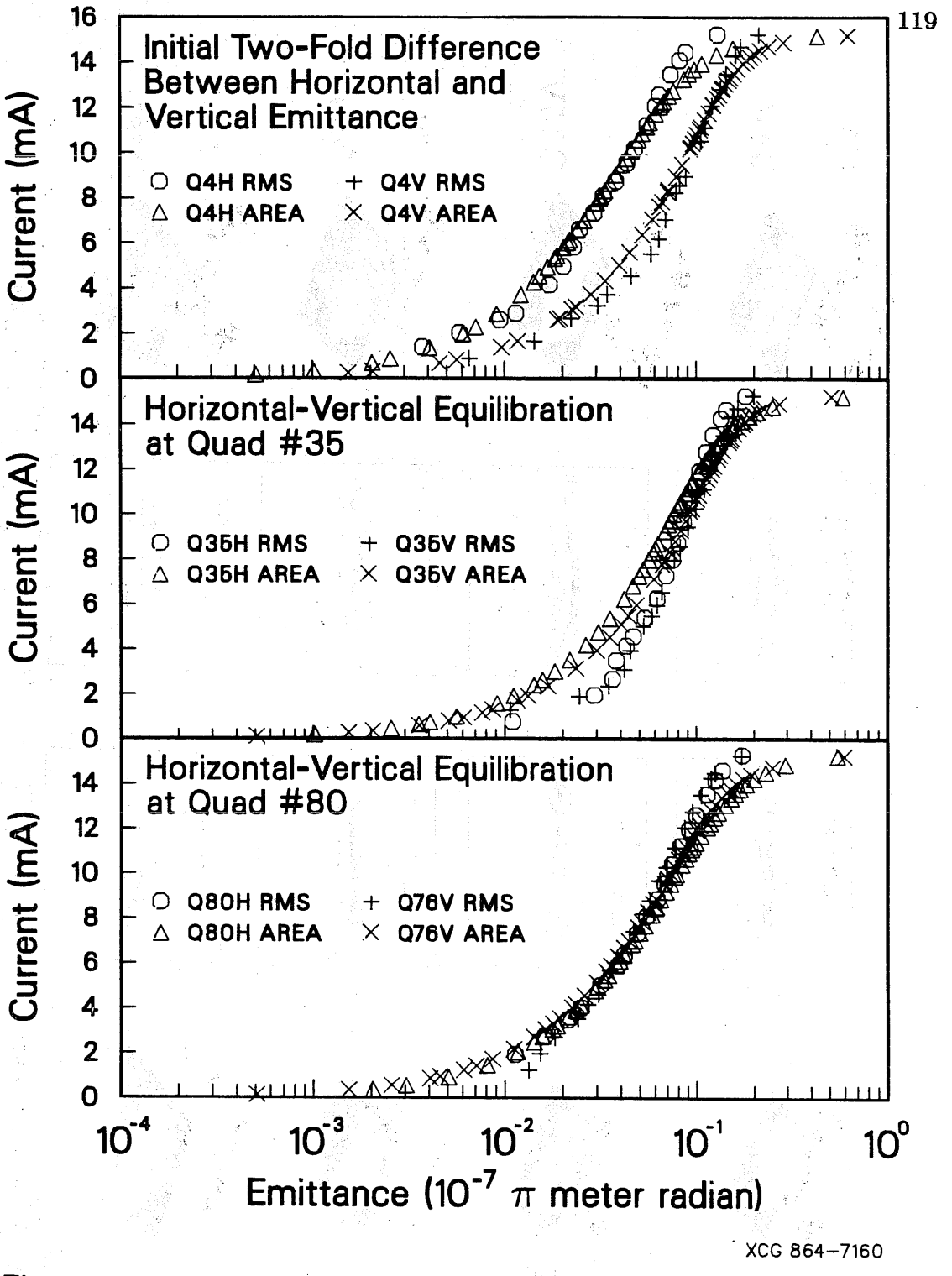

Figure 6.1: Horizontal-vertical emittance equilibration experimental results: (a) At Q4, the beam has almost a factor of 2 higher emittance in the vertical plane than in the horizontal plane. (b) By the time the beam has arrived at Q35, the transverse emittances are nearly equal. (c) The vertical emittance measured at Q76 and the horizontal emittance measured at Q80 are equal.

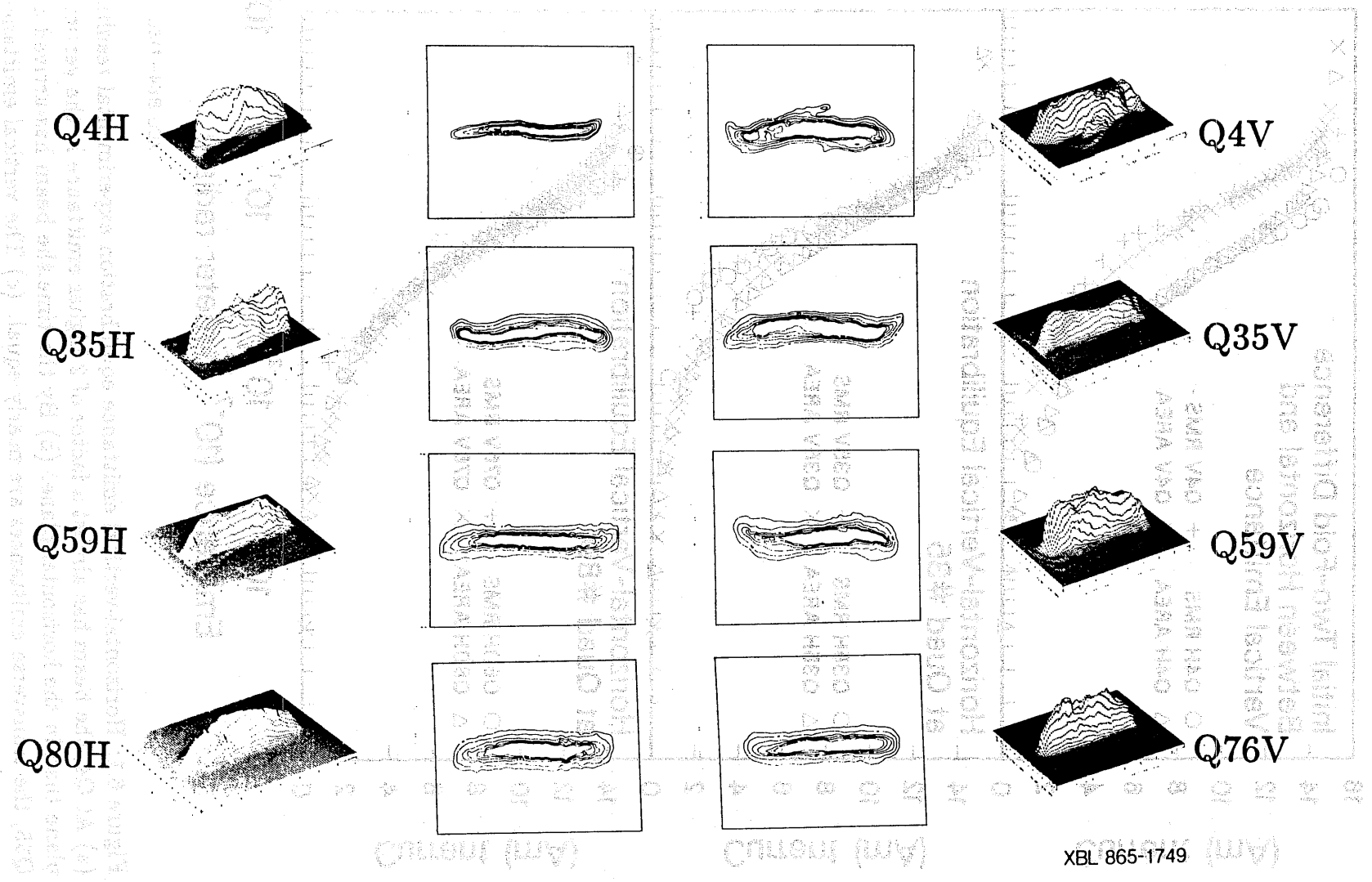

Figure 6.2: Phase space contours at various positions along the SBTE. The two left-most columns show the horizontal dimension results, while the two right-most columns show the vertical dimension data. The interchange of transverse energy is essentially completed upstream of Q35.

of 2 gives a final emittance in each plane of about 1.4, 1.5, or 1.6 times the smaller initial value. The final emittances in the two planes for the case of the horizontal grid orientation were equal to the emittances measured with the grid oriented at 45° to the horizontal.

6.2 Image Charge Effects

6.2.1 Shift in the coherent oscillation frequency

Other than collective instability of the phase space distribution of the beam, the emittance of a beam may be raised by the effect of induced charges on the quadrupole electrodes. Simulation results by Celata *et al.* [41] have indicated that induced charges on the quadrupole electrodes can raise the beam emittance greatly in the case of a misaligned beam, oscillating within the beamline, and Haber has shown that even for a well-aligned beam, the induced charges can limit the usable aperture [48]. At low values of the emittance, there is very little random thermal energy in the beam. The overall focusing provided by the lattice is almost totally cancelled by the space-charge defocusing. There is no real shielding of the beam interior by plasma-like redistribution of the particles, except for the average focusing over the lattice period. The nearly laminar beam flow can be vulnerable to the disturbing effects of relatively small driving terms, such as lens nonlinearities and image-charge fields.

To address this issue of image effects and make available a check on the accuracy of induced charge calculations in simulations, we have performed two experiments with the SBTE. The first effect we consider is the gross deflecting field experienced by the beam as it moves off-axis in the lattice. The induced field is very nonlinear, as may be seen from a first-order calculation using a cylindrical pipe for the aperture boundary. Treating the beam as a line charge with an offset d from the axis of the channel, there is an image line

charge as in Fig. 6.3. The image charge is of the same magnitude as the real charge, but with opposite sign, and lies a distance $R = a^2/d$ from the axis of the pipe, where the radius of the pipe is a. (The real, extended beam gives rise to an extended image of varying charge density.) The resulting field can be represented in first order as that due to a line image. The resulting field may be decomposed in the frame of the beam, into a dipole field (deflecting the beam) and higher-order multipoles, the magnitudes depending upon the beam offset. The dipole field, in particular, is a deflecting field of magnitude proportional to d in the small beam displacement limit, and causes a decrease of the coherent beam phase advance rate below the single particle rate. We denote this coherent phase advance rate by σ_C. Within the approximations above, treating the image of the beam as a line charge imaged by a cylindrical pipe surrounding the beam, in a constant-focusing channel, the image-charge shifted value for the coherent beam "tune" is given by

$$\sigma_C^2 = \sigma_0^2 - \left(2L\frac{180}{\pi}\right)^2 \frac{Q}{2a^2},$$

where $2L$ is the focusing period and Q is the generalized perveance. In the zero-current limit, $\sigma_C = \sigma_0$.

In the same way as we measured the single particle σ_0 (section 4.2), we measured the image-charge shifted phase advance rate σ_C for a 10-mA beam. We again set up the beam to have a zero-crossing after Q5, as we had for the low-current beam, and repeated the sequence of measurements. The results are shown in Fig. 6.4. For a quadrupole setting of 7275 volts ($\sigma_C = 59.2° \pm 0.6°$ for the low-current, 0.35-mA beam) we measured $\sigma_C = 55.2° \pm 0.6°$ for a 10-mA beam. The shift in σ_C due to the induced charges is thus $4° \pm 1°$ for $\sigma_0 \sim 60°$. The equivalent pipe radius which gives this same shift in the smooth focusing limit is about 34 mm, somewhat larger than the 25.4 mm

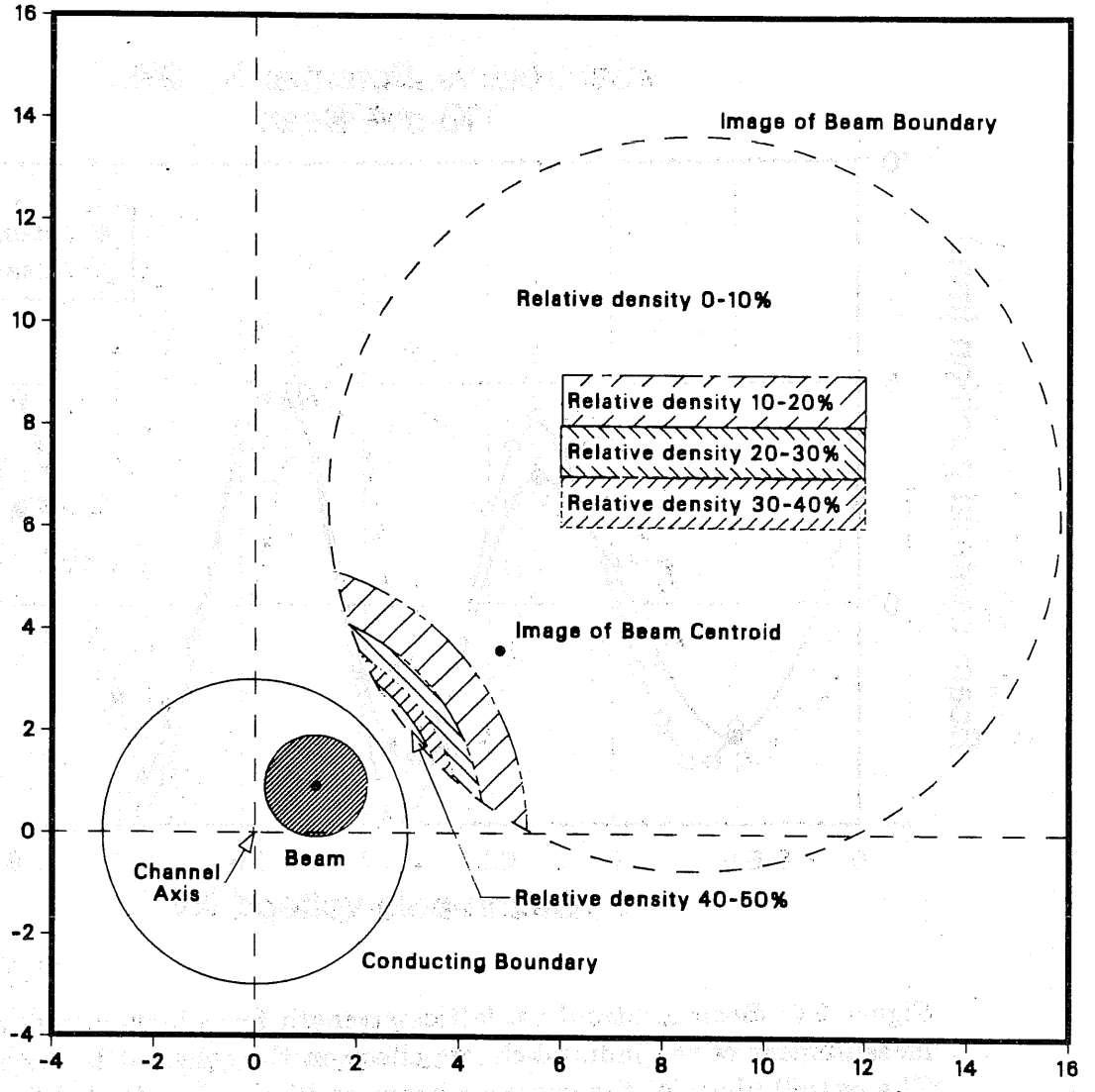

XBL 865-1842

Figure 6.3: Model treatment of induced charge as due a line image. Image forces may be treated approximately by replacing the nearby conductors with a conducting cylindrical pipe of some effective radius, a, and approximating the beam as a line charge of λ coulomb/meter. The image charge is then treated as an equivalent line charge, of density $-\lambda$ coulombs/meter, a distance a^2/d from the pipe axis, in the plane of the pipe axis and beam centroid. Here, d is the beam offset from the pipe axis. The actual image of the beam is more complex, as shown in the figure; the charge density of the image beam varies widely over the area of the image. The dipole component of the image field in the frame of the beam centroid has the approximate magnitude $(\lambda/2\pi\epsilon_0 a^2)d$, in the limit of d much less than a. This provides a linear deflecting force, which reduces the overall restoring force of the channel.

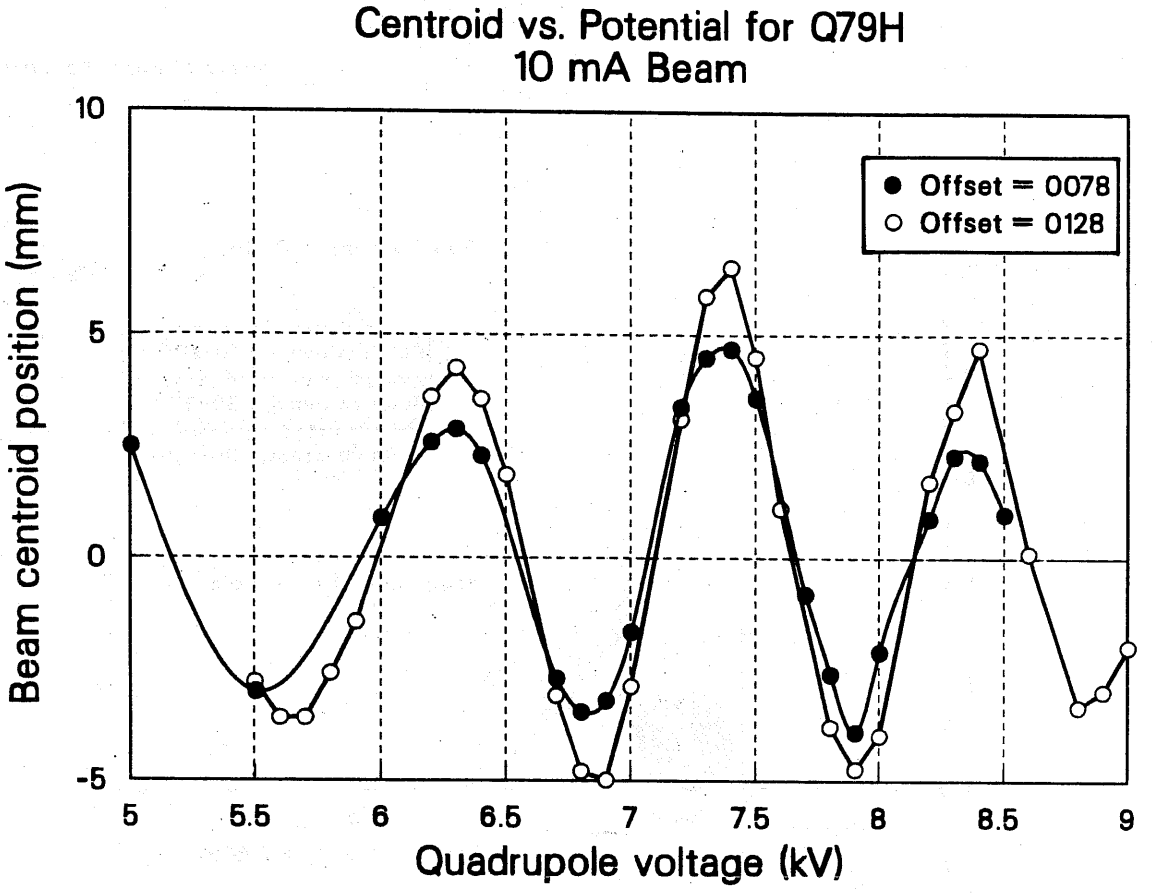

Figure 6.4: Beam centroid vs. lattice strength for a high-current beam, for measurement of the induced-charge effect on the coherent beam oscillation. The overall phase of the coherent beam oscillation is retarded from that of the low current case shown in Fig. 4.2. The shift for $\sigma_0 = 59°$ with respect to the low-current case in Fig. 4.2 is about $4° \pm 1°$, with a beam current of 10.3 mA and particle energy of 122.5 keV.

inner radius of the SBTE bore.

6.2.2 Emittance growth for off-axis beams

The higher order image multipoles also perturb the beam. The quadrupole term in the beam frame augments the net focusing provided by the lattice, but this is of minor importance. In simulation work by Celata *et al.* with off-axis beams, an oscillation of the beam was seen to be driven by the sextupole image field [41]. They assume that the beam is offset from the axis of a perfectly aligned quadrupole transport system, with the boundary surfaces for the induced charges provided by continuous electrodes with the same longitudinal projection as the SBTE quadrupoles described in Appendix D. This sextupole field can drive a sextupole-symmetry space charge oscillation, the frequency of which in the low-emittance, low-σ limit is degenerate with σ_0 [15]. The resulting time-varying perturbation to the beam distribution causes the RMS emittance to oscillate and grow in the simulation, as seen in Fig. 6.5. The beating shown in the figure is due to the difference between σ_C and the space-charge oscillation frequency. The simulations were run for $\sigma_0 = 60°$, and the effect was sensitive to the value of σ, being very serious for $\sigma \leq 6°$ and negligible for $\sigma \geq 12°$.

Our experiment in the SBTE has found qualitative agreement with this emittance growth. The SBTE diagnostics are not closely spaced enough to observe an oscillation in phase space, if present. The best alignment we can provide for the beam results in approximately a 1.5 mm offset of the beam centroid in the channel. By moving the quadrupole doublet Q1–2 off the beamline axis by about 0.04 in (this provision is part of the mechanism allowing insertion of the M5 DFC), we displaced the SBTE beam enough to cause a few percent of beam loss. This beam displacement is estimated to be about 3 mm. We compared the resulting 95% and 100% emittance

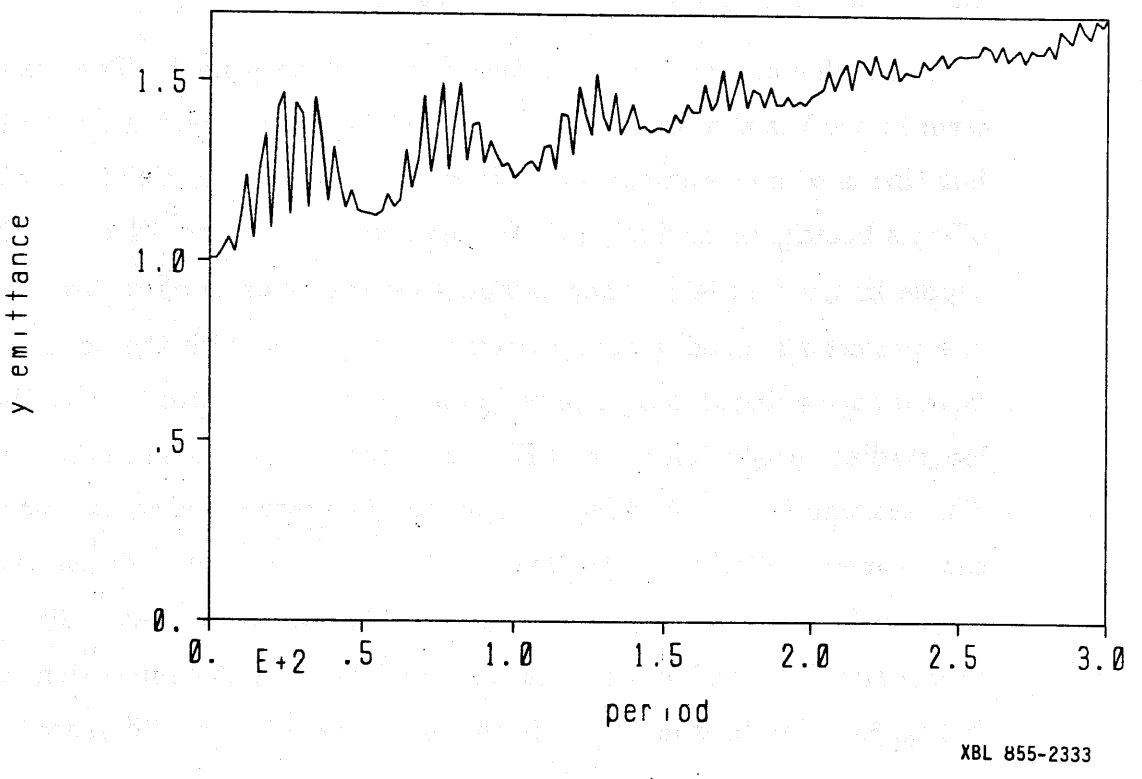

Figure 6.5: Simulation results for an offcenter high-current beam in a $\sigma_0 = 60°$ lattice, after Celata *et al.* The oscillation in emittance is due to a sextupole-symmetry space-charge oscillation with a frequency in the low-emittance limit that is nearly degenerate with σ_0. The image field, oscillating at σ_C, drives the oscillation. The beating visible in the figure is a result of the difference between the space-charge oscillation frequency and σ_C. The oscillation and growth in emittance are not present in simulation of a well-aligned beam.

values with those for the well-aligned beam, in both cases using the maximum current and minimum emittance attainable for us. The results are shown in Fig. 6.6. There is a small decrease in the apparent RMS emittance with z for the better-aligned beam, as mentioned in section 5.1.4. But with the added offset, the emittance grows somewhat even while some beam is lost. The beam current was 15 mA, with $2\tilde{x}$ calculated to be about 19 mm at the center of a focusing lens, an estimated maximum beam offset of about 3 mm within a quadrupole, and a mismatch oscillation amplitude of about 1–2 mm. This essentially uses all of the 25.4 mm bore radius. The offset used for the experiment was the largest we could provide while avoiding beam loss greater than a few percent.

The resulting roughly 10%–20% growth in RMS emittance in the experiment is comparable to that in the simulation results. If one assumes that the boundary may be represented by a conducting pipe, then the perturbation of a beam in a smooth focusing channel by the sextupole driving field is dependent on the pipe radius b, the beam radius a, and the offset h in the form a^3h^3/b^4, as shown in [41]. The expected perturbation in phase space, and consequently the emittance growth rate, depend strongly on the offset, which is not well-specified in the experiment. Because of the inevitable misalignments in the lenses, the phase and amplitude of the coherent beam oscillation will shift with respect to those for the perfect lattice alignment of the simulation. The relative phases of the space-charge oscillation and the coherent oscillation will therefore have a relative drift other than that which gives rise to the orderly beating of the simulation.

6.3 Background Gas Stripping of Cs^+

Another possible source of spurious beam loss and emittance growth in the SBTE is that the Cs^+ ions may change their charge state during collisions

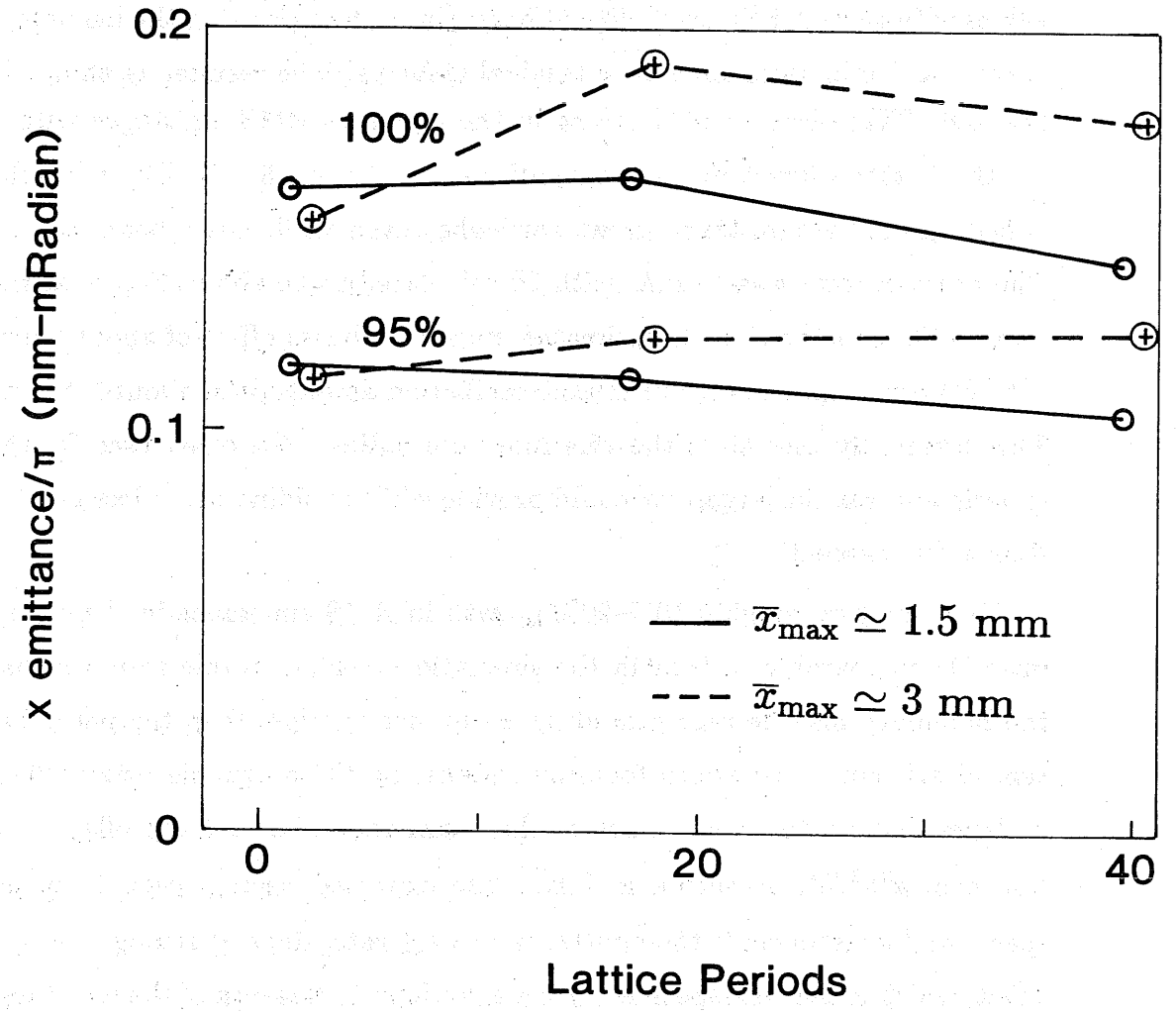

XBL 854-2195

Figure 6.6: Experimental emittance growth for high-current, off-center beam. Sparseness of diagnostics would not permit detection of any oscillation in the emittance. The best alignment possible results in a beam offset within the bore of about 1.5 mm, due to the lattice alignment errors. For the well-aligned beam, the measured emittance decreases slightly along the lattice. By shifting the Q1–2 doublet horizontally about 1 mm from its former position, we increase the offset of the beam within the channel to about 3 mm. We observe a few percent loss of current at the Q82 DFC, and a rise in the emittance of the remaining beam. The roughly 10–20% growth in emittance is consistent with the simulation result.

with background gas molecules. Any neutrals will be lost to the beam, resulting in beam loss without growth in the emittance. However, Cs^{+2} ions can be retained in the lattice under certain experimental conditions and be detected by the diagnostics. Because their orbits will be grossly different from those of the Cs^{+} ions, retained Cs^{+2} ions will show up as a halo of particles in phase space. The result would be indistinguishable from a collective degradation of the Cs^{+} beam emittance, and we must determine the possible magnitude of this effect.

Typical stripping cross-sections are on the order of a few times 10^{-16} cm^2 [49], and if we estimate the probability of stripping (or neutralization) over the length of SBTE ($l = 13$ meter) at a pressure of 5×10^{-7} Torr, assuming that the cross-section is on the order of $\sigma \sim 10^{-16}$ cm^2, we obtain $n\sigma l \sim .002$, where n is the number density of the gas molecules and l is the length of the channel. We may safely assume that the ions will undergo at most one charge-state changing collision, and we may use the transmitted beam current to determine the actual neutralization and stripping cross-sections (which we will denote, respectively, by σ_{10} and σ_{12}).

For σ_0 somewhat greater than 60° for a Cs^{+}, the corresponding σ_0 for a Cs^{+2} is beyond the 180° single-particle stability threshold, as may be seen from Fig. D.3 in Appendix D. The energy and transverse velocity of an ion change negligibly during stripping, though its charge doubles. This means that the Cs^{+2} suddenly experiences forces corresponding to a doubled lens strength, but with initial conditions appropriate for a Cs^{+}. In the zero-current limit, these particles will be driven from the beam, and the current along the lattice will vary as

$$I = I_0 \exp[-(\sigma_{10} + \sigma_{12})nz],$$

where z is the distance along the channel. (However, in the presence of the signficant space-charge forces of an intense Cs^+ beam, many of the Cs^{+2} ions can be stable in the weakened net focusing field.) For much weaker focusing, with a beam clearance sufficient to accommodate the mismatched initial conditions for the Cs^{+2}, these ions would be retained. The current in this regime would vary as

$$I = I_0 \exp[-(\sigma_{10} - \sigma_{12})nz],$$

because the σ_{12} interactions increase the electrical current of the beam.

We measured transmitted current as a function of lattice voltage and gas pressure for low-current beams for both 160 keV operation and 120 keV operation. We varied the pressure by opening a leak valve connected to atmosphere. The measured cross sections thus are appropriate to approximately $80\%N_2 - 20\%O_2$ gas. The results, in terms of fractional beam transmission for the other parameters, are shown in Figs. 6.7 and 6.8. From the slopes of the curves using a lattice strength above that for which the doubly-charged ions can remain in the lattice, we calculate the sum of the cross-sections σ_{10} and σ_{21}. Note that in Fig. 6.7, the initial slopes of the very low quadrupole strength curves is positive, indicating that second ionization occurs more often than neutralization, even allowing for incomplete retention of the Cs^{+2} ions. The electrical current of the beam rises, even as the particle current drops.

For strengths far from that for which the beamlet was matched, this will be a lower current than measured for a matched beam. In Fig. 6.7 (120 keV ions), for a quadrupole voltage less than about 3 kV, only part of the beam is transported to the Q82 Faraday cup. If the Cs^+ ions are aperture limited, then so will the Cs^{+2} be, and the value we obtain for $\sigma_{10} + \sigma_{12}$ will be an underestimate. In this parameter range, the overlap of the Cs^+ and Cs^{+2}

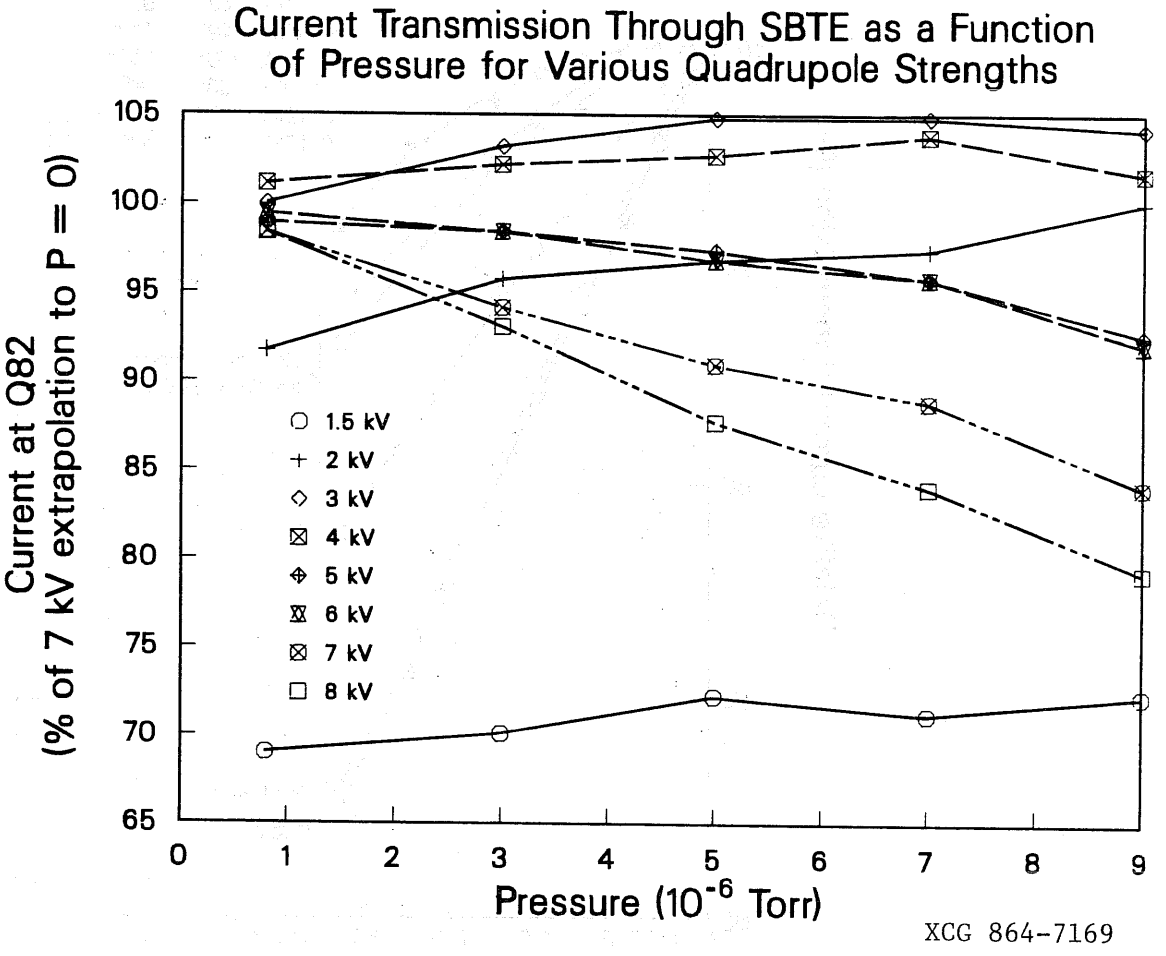

Figure 6.7: Current vs. pressure in SBTE lattice at 120 keV particle energy. Second ionization of the Cs^+ ions causes loss of the ion for quadrupole voltages above about 7.5 kV, because $\sigma_0 > 180°$ for the resulting Cs^{+2} ion. For lower quadrupole voltages, a Cs^{+2} ion may remain, if its transverse phase space coördinates fall within the acceptance curve for the new charge state. The exponential loss of ions from the beam from the combined processes of second ionization and neutralization may be calculated from the high voltage current vs. pressure curves. If the bore clearance is great, so that all the Cs^{+2} are retained, the low voltage curves give the exponential drop (or rise) in current as the electrical current is augmented by the Cs^{+2} ions. If the second ionization rate exceeds the neutralization rate, the current rises with pressure until the depopulation of Cs^{+2+} ions by other processes becomes important. The very low voltage curves for the 120 keV ions show a distinct rise in current at the Q82 Faraday cup, as the pressure rises. This effect disappears for quadrupole voltages greater than about 4 kV.

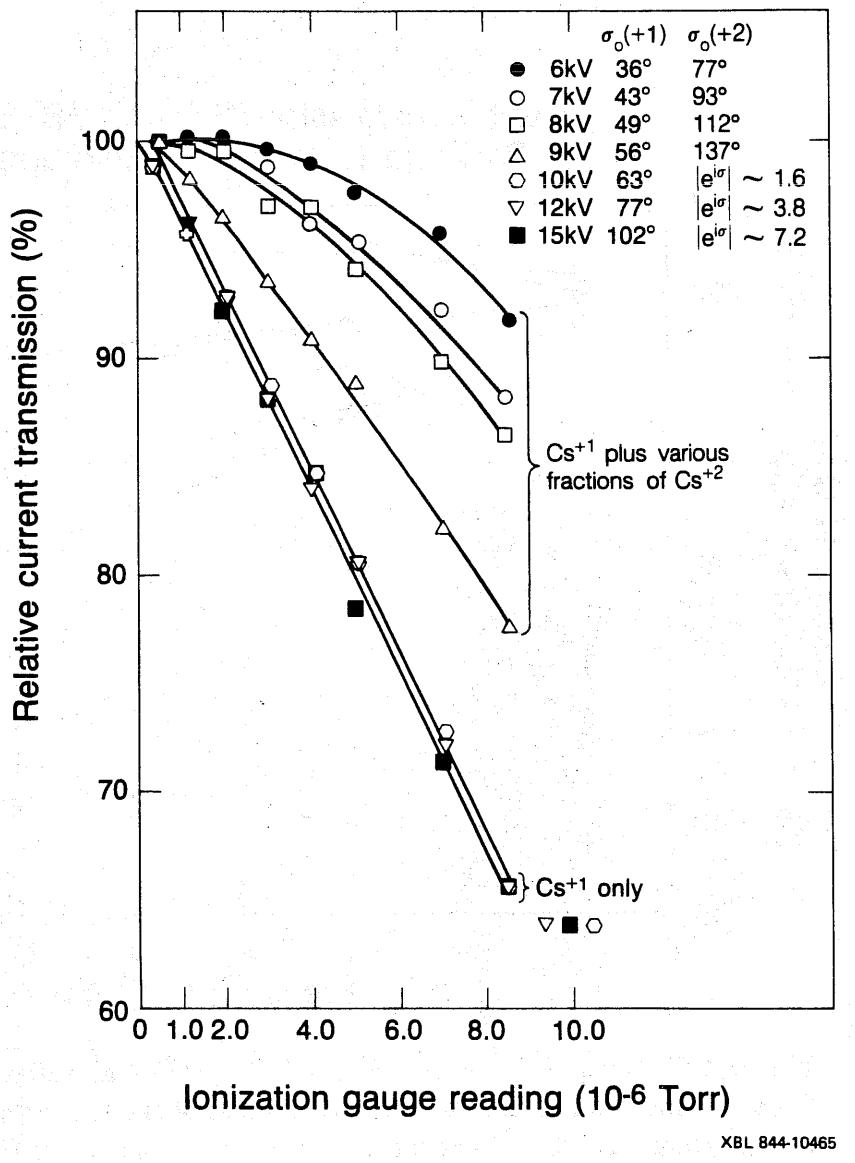

Figure 6.8: Current vs. pressure in SBTE lattice at 160 keV particle energy for various lattice strengths. The 6 kV minimum quadrupole potential shown for 160 keV ions corresponds to 4.5 kV for 120 keV ions. Based on the results for 120 keV ions, our measurements for the 160 keV case were not carried to quadrupole strengths low enough to measure the difference in the second ionization and neutralization cross-sections. We expect the difference in cross-sections to be comparable for 120 keV and 160 keV ions.

	Measured cross sections (10^{-16} cm^2)	
	120 keV	160 keV
$\sigma_{12} + \sigma_{10}$	5.2 ± 0.5	9.2 ± 0.7
$\sigma_{12} - \sigma_{10}$	2.0 ± 0.7	2 ± 2 (est.)
σ_{12}	3.6 ± 0.6	5.6 ± 1.4
σ_{10}	1.5 ± 0.6	3.6 ± 1.4

Table 6.1: Measured cross-sections for charge-changing collisions for 120 and 160 keV Cs^+ ions against air.

acceptances of the lattice is good, so most of the stripped ions will be retained. For $V_Q \sim 4$ kV, the current becomes flat with pressure, because the overlap in the lattice acceptance for the two species decreases. By extrapolating the curves to zero pressure, we determine how much current would have been transmitted by the lattice in the absence of charge-changing collisions. This is the base current that should be used to calculate the relative change in current with pressure for each particular lattice voltage. We have instead plotted the curves as the fraction of the maximum zero-pressure beam current (about 0.37 mA) to show the incomplete transmission for low lattice strength which results from severe mismatch of the beam. For the 160 keV beam in Fig. 6.8, we did not extend the measurements to a low enough lattice strength to get a good measurement of the difference of the cross-sections, although we can measure the sum of the cross-sections. We estimate from the rough equality of the slopes of the 6 kV quadrupole voltage for 160 keV ions and of the equivalent line interpolated for 4.5 kV quadrupole voltage and 120 keV ions, that the difference of the cross-sections for 160 keV ions is about the same as for the 120 keV ions. Our final results are given in Table 6.1.

Using 9×10^{-16} cm^2 for the sum of the cross sections, we see that for an indicated pressure of 5×10^{-7} Torr, at most 2% of the beam particles

undergo a charge-state changing collision. This is small enough to neglect in our emittance measurements, particularly since we quote emittance values for the most intense 95% of the beam.